

# Integrating Chemical Language and Molecular Graph in Multimodal Fused Deep Learning for Drug Property Prediction

Xiaohua Lu<sup>1</sup>, Liangxu Xie<sup>1,\*</sup>, Lei Xu, Rongzhi Mao<sup>1</sup>, Shan Chang<sup>1,\*</sup>, Xiaojun Xu<sup>1,\*</sup>

<sup>1</sup>Institute of Bioinformatics and Medical Engineering, School of Electrical and Information Engineering, Jiangsu University of Technology, Changzhou 213001, China.

Corresponding authors: L.X.: [xieliangxu@jsut.edu.cn](mailto:xieliangxu@jsut.edu.cn); S.C., [schang@jsut.edu.cn](mailto:schang@jsut.edu.cn); X.X. [xuxiaojun@jsut.edu.cn](mailto:xuxiaojun@jsut.edu.cn).

**Abstract:** Accurately predicting molecular properties is a challenging but essential task in drug discovery. Recently, many mono-modal deep learning methods have been successfully applied to molecular property prediction. However, the inherent limitation of mono-modal learning arises from relying solely on one modality of molecular representation, which restricts a comprehensive understanding of drug molecules and hampers their resilience against data noise. To overcome the limitations, we construct multimodal deep learning models to cover different molecular representations. We convert drug molecules into three molecular representations, SMILES-encoded vectors, ECFP fingerprints, and molecular graphs. To process the modal information, Transformer-Encoder, bi-directional gated recurrent units (BiGRU), and graph convolutional network (GCN) are utilized for feature learning respectively, which can enhance the model capability to acquire complementary and naturally occurring bioinformatics information. We evaluated our triple-modal model on six molecule datasets including Delaney, Llinas2020, Lipophilicity, SAMPL, BACE, and pKa from DataWarrior. Different from bi-modal learning models, we adopt five fusion methods to capture the specific features and leverage the contribution of each modal information better. Compared with mono-modal models, our multimodal fused deep learning (MMFDL) models outperform single models in accuracy, reliability, and resistance capability against noise. Moreover, we demonstrate its generalization ability in the prediction of binding constants for protein-ligand complex molecules in the refined set of PDBbind. The advantage of the multimodal model lies in its ability to process diverse sources of data using proper models and suitable fusion methods, which would enhance the noise resistance of the model while obtaining data diversity. Multimodal fused deep learning model can accurately predict molecular properties by extracting comprehensive and complementary information from each modal and we expect its successful applications in drug discovery.

**Keywords:** Multimodal learning; deep learning; drug discovery; Transformer; Graph

## Introduction

Drug discovery has historically been costly with low success rates<sup>[1]</sup>. Many factors need to be considered for successful drug discovery, including solubility<sup>[2]</sup>, lipophilicity<sup>[3]</sup>, inhibitory activity<sup>[4]</sup>, acidity/basicity<sup>[5]</sup>, and assessing protein-ligand binding affinity<sup>[6]</sup>. Experimental determination is often expensive and time-consuming. Accurate prediction of drug properties is a crucial aspect of drug discovery<sup>[7]</sup>. Computational methods have been established to assist drug discovery, including physics-based and machine learning-based methods. Physics-based computational methods have been developed, including molecular docking<sup>[8]</sup>, molecular dynamics simulations<sup>[9]</sup>, and quantitative structure-activity relationships (QSAR)<sup>[10]</sup>. These methods aim to explain molecular-related properties and have made great contributions to drug research and development. These methods show their strength in examining molecular structure, interaction, and motion. However, the physics-based methods face challenges, including computational complexity, high resource requirements, and reliance on experimental data<sup>[11]</sup>. With the improvement of computer performance and calculation methods, deep learning methods have emerged and achieved notable success in predicting drug properties<sup>[12-15]</sup>.

To apply deep learning to drug property prediction, molecules need to be transformed into molecular descriptors. Researchers have explored various representation methods, including Simplified Molecular Input Line Entry System (SMILES), extended connectivity fingerprints (ECFP), molecular graphs, etc. The application of molecular fingerprinting in machine learning models has effectively improved QSAR prediction performance<sup>[16]</sup>. For example, Karimi et al. constructed the DeepAffinity model using integer encoding for (SMILES) and numeric encoding for amino acid sequences<sup>[17]</sup>. ECFP is one type of topological-based method that converts the neighborhood information into bit strings. ECFP and its variants have been widely used in bioinformatics and drug discovery<sup>[18]</sup>. SMILES-encoded vectors and ECFP are numerical representations used to encode chemical structures. They can be considered as the chemical language. To capture the whole topology of molecules, another type of molecular representation called molecular graph is proposed. In molecular graphs, atoms are described as nodes, and bonds are represented as edges. Various graph neural networks (GNN) have been employed to process molecular graphs, including message-passing neural network (MPNN)<sup>[19]</sup> and variants with attention mechanisms<sup>[20, 21]</sup> to predict molecular properties. Different molecular representations provide particular types of information. Interdisciplinary work is required to obtain the specific information conveyed from molecular representations.

Though previously reported methods have made progress using single-input modes or single models, unimodal learning suffers from incomplete information representation. Unimodal learning exhibits dependence on dataset and model selection. To enhance the expressiveness of existing molecular representations, combined molecular representation learning methods, multi-task learning and ensemble methods have been

developed [22-27]. Currently, multi-modal learning is a vibrant multidisciplinary field, which provides another framework to process multiple sources of information<sup>[28, 29]</sup>. Multimodal learning is a general approach for constructing artificial intelligence models that can extract and associate information from multimodal data, enabling models to handle complex relationships between different modalities<sup>[30, 31]</sup>. The rich and diverse information in multimodal data is essential for drug property prediction<sup>[32]</sup>. Pioneering works have been conducted recently. For example, Dong et al. designed the multimodal attribute learning framework (MMA-DPI) using molecular transformer and graph convolutional networks for predicting drug-protein interactions, and experimental results showed that the proposed method achieved higher performance than the existing advanced frameworks<sup>[33]</sup>. Sun et al. proposed bi-modal representations for protein-protein interactions, which achieved higher screening ability<sup>[34]</sup>.

Multimodal approaches have not been widely applied in the field of drug properties because most of the studies in this field use a single model. There is no practical approach to leverage or balance contribution from different modalities because the information can exist as redundant, complementary, or cooperative<sup>[35]</sup>. Existing multimodal techniques include early and late fusion<sup>[36]</sup>, hybrid fusion, model ensemble<sup>[37]</sup>, and more recently, joint training methods based on deep learning networks<sup>[38, 39]</sup>. Multimodal systems need to ingest, interpret, and reason from multiple modal information sources. Therefore, multimodal methods pose challenges, including the representation of multimodal data, modality transformations, measuring relationships between different modalities, integrating modality information, and transferring knowledge between modality information and their predictive models. Several attempts have been made to address the challenges. To filter noise while capturing synergies from different modalities, Liu et al. proposed a novel penalty-modality method, making decisions independently for each modality first, and then completing a multimodal combination in a differentiable or multiplicative manner, which effectively improves the accuracy of the prediction<sup>[40]</sup>. Yang et al. also emphasize the importance of the fusion strategy<sup>[41]</sup>. Dehghan et al. propose a triplet loss function in the processing of multimodal representation learning<sup>[42]</sup>.

Designing a multimodal deep learning method suitable for drug property prediction holds significant promise to enhance the accuracy of existing computational approaches and broaden their applicability, presenting important prospects for practical applications. In this study, we proposed a triple-modal fusion learning method to predict molecular properties. Two major contributions of this study are summarized as follows,

- We employed Transformer-Encoder, BiGRU, and GCN models to process SMILES-encoded vectors, ECFP, and molecular graph. In bioinformatics, molecules can be represented by three different and complementary representations. The proposed multimodal fused deep learning model can harness the diverse information while fully utilizing the advantage of the deep learning models.
- To combine information from multimodal features, we follow the idea of previous report<sup>[40]</sup>, but instead of the multiplicative combination method, we adopt four machine learning methods (LASSO, Elastic Net, Gradient boosting

(GB) and random forest (RF)) and one numerical way of stochastic gradient descent (SGD) to assign the contributions for each modal learning.

We compared the performance of the constructed multimodal fusion deep learning (MMFDL) model with single modal models in predicting drug properties. Experimental results indicate that our constructed multimodal fusion deep learning model (MMFDL) contributes to improved predictive performance and also increased generalization ability and enhanced noise resistance.

## Materials and methods

### Datasets

We evaluated the proposed models on six single-molecule drug property datasets and one protein-ligand complex molecule dataset, including Delaney, Llinas2020, Lipophilicity, SAMPL, BACE, pKa from DataWarrior, and the refined set of PDBbind<sup>[43, 44]</sup>. Among these, solubility is a measure of a drug's ability to be absorbed in the gastrointestinal tract, related to the distribution and elimination of the drug in the body. Lipophilicity is typically associated with a drug's membrane permeability and distribution, impacting the drug's penetration and absorption in cell membranes. Inhibition activity from BACE measures a crucial indicator of the therapeutic potential of a drug. The acidity/basicity of a molecule forms the basis for many critical processes in chemical and biological systems. Moreover, we demonstrate the generalization ability of multi-modal using the refined set of PDBbind2020. Protein-ligand binding affinity is used to measure the strength of interactions between drugs and proteins, a property crucial for understanding the biological activity and effects of drugs.

(a) Delaney is a dataset for molecular solubility, comprising the chemical structures and corresponding experimentally measured solubility data for 1128 small molecules<sup>[43]</sup>. All solubility values are expressed in units of  $\log_{10}(\text{mol/L})$ .

(b) Llinas2020 dataset is derived from the SolTransNet dataset<sup>[45]</sup>. The training set contains 9860 molecules and the test set of Llinas2020 has 100 molecules with solubility values.

(c) Lipophilicity is a lipophilic dataset from MoleculeNet, consisting of LogP values and SMILES for 4200 molecules<sup>[43]</sup>.

(d) The SAMPL dataset from MoleculeNet is a statistical evaluation dataset for protein and ligand modeling and consists of 642 experimental values  $\log P$ <sup>[43]</sup>.

(e) BACE is a dataset on the activity of compounds against  $\beta$ -secretase and contains data on the activity of 1513 compounds against  $\beta$ -secretase<sup>[43]</sup>. The inhibitory activity of molecules is explored using pIC50 from the BACE dataset. pIC50 is commonly used in chemical and biological research to represent concentration-effect relationships.

(f) pKa data provided by the DataWarrior visualization software proposed by Sander et al. and contains 7910 data related to pKa. pKa describes the acidity/basicity of a molecule in water, and this metric involves the ionization equilibrium in aqueous



## SMILES tokenization and vectorization

SMILES is a line symbol that represents the atoms, bonds, and rings that make up a molecule as a string. SMILES show effective applications, including fast search and substructure search. In tokenization, each atom is represented by an alphabet of elemental symbols<sup>[46]</sup>. These bonds are represented by different symbols for single (-), double (=), triple (#), and quadruple (\$) bonds, and a detailed specification of SMILES can be found in OpenSMILES<sup>[47]</sup>. The type of bond can be easily inferred by the ring structure of the atom or surrounding atoms. For example, the six-carbon ring molecule benzene can be represented by "C1=CC=CC=C1", where "=" represents a double bond and "1" signifies a ring or the beginning/end of a cycle. SMILES tokenization and vectorization are revised based on custom regular expressions that can capture 'single atom' type, 'double bond' type, 'triple bond' type etc. For example, the SMILES string 'CS(=O)(=O)Cl' uses regular expressions and can be split into a list of ['C','S','(','=','O',''),'(','=','O',''),'Cl']. Converting molecular structural information into numerical form facilitates a variety of tasks.

For different datasets, a unified regular expression is used to construct a label dictionary. The SMILES in the dataset are mapped to fixed-length integer sequences by the labeling dictionary (the length distribution of SMILES strings see Figure S1 in SI). Every token in the SMILES sequence is subjected to encoding, followed by the generation of an embedding vector for each token. Any shorter SMILES strings were padded with zeros at the end. The length of SMILES-encoded vectors in different data is shown in Table 1. The finally generated embedding vector is used as the input of Transformer-Encoder.

Table 1 Encoding length of molecules in different datasets

	Delaney	Llinas 2020	Lipophili city	SAMPL	BACE	Warrior	PDBbind 2020 refined
SMILES- encoded vectors	130	230	100	44	130	64	1530
ECFP Fingerprint	1024	1024	1024	1024	1024	1024	2048

## ECFP Fingerprints

ECFP is a circular topological fingerprint that uses circular atomic neighborhoods to generate variable-length hashed integer identifiers, with each unique identifier corresponding to a unique substructure of the compound. This approach describes a complex as a fixed-length bit string, with each bit indicating the presence or absence of a particular substructure in the complex. This fingerprinting method<sup>[48]</sup> can be used for structure-activity modeling, Quantitative Structure-Activity Relationship (QSAR) analysis, and drug ADME/T prediction. The extension radius can be customized and

commonly used diameters are 4, 6, and 8. Several software programs providing fingerprints include Pipe-line Pilot, Chemaxon's JChem<sup>[49]</sup>, CDK<sup>[50]</sup>, and RDKit<sup>[51]</sup>. In this study, we adopt RDKit to convert molecules into fingerprints. The lengths of ECFP fingerprints in different datasets are shown in Table 1.

## Graph

We represent molecules as graphs to obtain more accurate structural information about the molecules<sup>[52]</sup>. A molecular graph can be formulated as  $G = (V, E)$ , where  $V \in R_n \times f$  is a set of  $n$  atomic nodes, with each node represented by a feature vector composed of 78 values, including 44 atomic types, 11 one-hot encoding atom degree, 11 one-hot encoding of the total number of hydrogens, 11 one-hot encoding valences and 1 bit for the aromaticity.  $E \in R_n \times n$  is the set of edges represented by the adjacency matrix of the molecular graph. The existence of an edge in an adjacency matrix depends on whether there are direct covalent chemical bonds between the corresponding atoms in the molecule.

## Construction of multimodal model

The overall framework of our proposed multimodal model is illustrated in Figure 2. Our task involves predicting the solubility, lipophilicity, molecule inhibitory activity, and protein-ligand binding affinity. As depicted in Figure 2(A) for learning different representation features, we use two identical primitive Transformer-Encoders for the SMILES-encoded vectors, and the output is sent to the fully connected layer. As shown in Figure 2(B), for learning ECFP fingerprint features, we send the ECFP through two layers of BiGRU to the fully connected layer. As shown in Figure 2(C), for learning molecular graph information, we use the graph's adjacency matrix and feature vectors as input, employ two GCN layers with corresponding activation functions, average pool  $t$ , and connect to a fully connected layer to obtain the output. We use the training set to train the model for extracting features and the validation set for evaluating the hyperparameters of the feature extraction model. To calculate the weights of the each modal features during fusion stage, we use the specific data set named tuning set, which uses the data in the validation set. We compute the weights of the different models after splicing the three learned multimodal feature outputs using five methods based on machine learning methods and numeric method for combination, which are referred to as Tri\_LASSO, Tri\_Elastic, Tri\_RF, Tri\_GB, and Tri\_SGD by using LASSO, Elastic Net, RF, GB and SGD. Finally, on the test set, we predict the properties for different tasks using assigned weights.

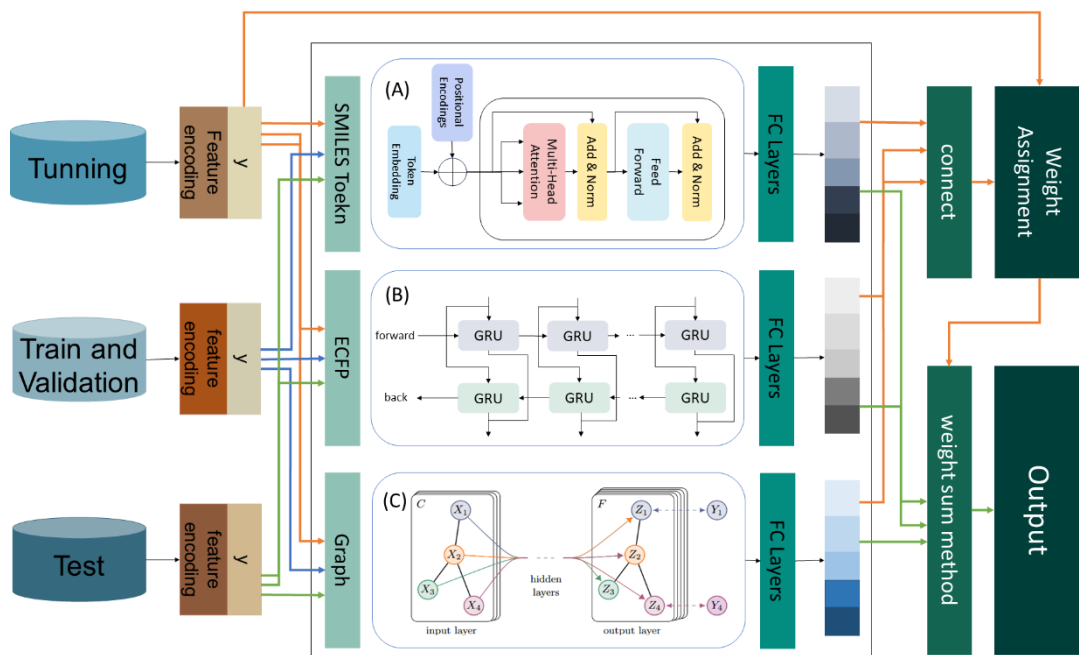


**Figure 2** The overall structure of the multimodal fused deep learning (MMFDL) model. Blue, orange and green color lines represent the data flow in the model for training, tuning, and test sets. SMILES-encoded vectors are processed by Transformer-Encoder, ECFP is processed by BiGRU, and Graph is processed by GCN model. The training set is used to train the feature extraction model; the validation set determines the hyperparameters of the feature extraction model. The tuning set is used to assign the weights for each modal input. The test set is used to validate the prediction performance.

### Transformer-Encoder

The Transformer encoder<sup>[53]</sup> consists of a stack of identical layers, and each Transformer encoder layer is composed of a multi-head self-attention sub-layer followed by a position-wise feedforward sub-layer. For the molecule representation  $X$ , after token embedding and position encoding, it is passed through the encoder to extract features for molecular property prediction. First, let input  $X$  for token embedding and obtain the embedding vector  $P \in R^{l \times d}$ . To retain position information, sinusoidal positional embeddings PE are added to the embedding vector  $P$ . This position encoding introduces a position-invariant trigonometric signal to locate different elements of the token embedding sequences<sup>[53]</sup>.

$$PE_{(pos,2i)} = \sin\left(\frac{pos}{10000^{\frac{2i}{d}}}\right) \quad (1)$$

$$PE_{(pos,2i+1)} = \cos\left(\frac{pos}{10000^{\frac{2i}{d}}}\right) \quad (2)$$

where  $pos$  is the position and  $i$  is in the range of  $\left[0, \frac{d}{2}\right]$ ,  $d$  is the input dimension. This sinusoid-based position embedding gives Transformer the ability to model the position of a token and the distance of each two tokens. For any fixed offset  $k$ ,  $PE_{pos+k}$  can be represented as a linear function of  $PE_{pos}$ .

The transformer encoder takes in a matrix  $H \in R^{l \times d}$ , where  $l$  is the molecular sequence length,  $d$  is the input dimension. Then three learnable matrix  $W_q, W_k, W_v$  are used to project  $H$  into different spaces. Usually, the matrix size of the three matrices is all  $R^{d \times d_k}$ , where  $d_k$  is a hyper-parameter. After that, the scaled dot product attention can be calculated by the following equations<sup>[54]</sup>.

$$Q, K, V = HW_q, HW_k, HW_v \quad (3)$$

$$\text{Attention}(Q, K, V) = \text{softmax}\left(\frac{QK^T}{\sqrt{d_k}}\right)V \quad (4)$$

We use several groups of  $W_q^{(h)}, W_k^{(h)}, W_v^{(h)}$  to enhance the ability of self-attention. When several groups are used, it is called multi-head self-attention, the calculation can be formulated as follows<sup>[54]</sup>.

$$Q^{(h)}, K^{(h)}, V^{(h)} = HW_q^{(h)}, HW_k^{(h)}, HW_v^{(h)} \quad (5)$$

$$\text{head}^{(h)} = Q^{(h)}, K^{(h)}, V^{(h)} \quad (6)$$

$$\text{MultiHead}(H) = \left[ \text{head}^{(1)} \dots \text{head}^{(n)} \right] W_o \quad (7)$$

where  $n$  is the number of heads, the superscript  $h$  represents the head index.  $\left[ \text{head}^{(1)} \dots \text{head}^{(n)} \right]$  means concatenation in the last dimension. Usually  $d_k \times n = k$ , which means the output of  $\left[ \text{head}^{(1)} \dots \text{head}^{(n)} \right]$  will be of size  $R^{l \times d}$ .  $W_o$  is a learnable parameter, which is of size  $R^{d \times d}$ .

The output of the multi-head attention will be further processed by the position-wise feedforward networks, which can be represented as follows<sup>[54]</sup>.

$$\text{FFN}(x) = \max(0, xW_1 + b_1)W_2 + b_2 \quad (8)$$

where  $W_1, W_2, b_1, b_2$  are learnable parameters, and  $W_1 \in R^{d \times d_{ff}}$ ,  $W_2 \in R^{d_{ff} \times d}$ ,  $b_1 \in R^{d_{ff}}$ ,  $b_2 \in R^d$ .  $d_{ff}$  is a hyper-parameter.

Transformer-Encoder takes the self-attention mechanism as its core, and can pay attention to all positions in the sequence at the same time. SMILES-encoded vectors perform integer mapping on atoms and bonds in molecules, allowing the structure and properties of molecules to be expressed in digital form and can be considered as the chemical language. The Transformer-Encoder enables a more comprehensive capture of molecular structure information by extracting SMILES-encoded vectors.

## BiGRU

We use BiGRU to capture substructure information of molecules. The main idea of GRU is to make every recurrent unit to adaptively capture dependencies of different time scales. GRU is composed of an update gate and a reset gate and has the advantages of a simpler structure, fewer parameters and better convergence. Let  $X = (x_1, x_2, \dots, x_t)$  be the input sequence, where  $x_t \in R^d$ . The current hidden state  $h_t^i$  of each GRU unit at a time  $t$  is a linear interpolation between the previous hidden state  $h_{t-1}^i$  and the candidate hidden state  $h_t^i$ . The current hidden state  $h_t^i$ , the candidate state  $h_t^i$ , the update gate  $z_t^i$  and the reset gate  $r_t^i$  are calculated as follows<sup>[55]</sup>.

$$h_t^i = (1 - z_t^i)h_{t-1}^i + z_t^i h_t^i \quad (9)$$

$$h_t^i = \Phi(Wx_t + U(r_t \odot h_{t-1}^i))^i \quad (10)$$

$$z_t^i = \sigma(W^z x_t + U^z h_{t-1}^i)^i \quad (11)$$

$$r_t^i = \sigma(W^R x_t + U^R h_{t-1}^i)^i \quad (12)$$

where  $\Phi$  and  $\sigma$  represent different activation functions (i.e. ‘tanh’ and ‘Sigmoid’),  $W, W^z, W^R, U, U^z, U^R$  represent the corresponding weight coefficients. An update gate  $z_t^i$  regulates how much the recurrent unit computes its hidden state and a reset gate  $r_t^i$  represents a set of reset gates;  $\odot$  is an element-wise multiplication.

Due to GRU not encode information from back to the front, it may affect the acquisition of potential relationships between the current character in the ECFP fingerprints and its surrounding chemical information. Therefore, we adopt a BiGRU, instead of using directly the GRU neural network mentioned earlier. The BiGRU processes the input sequences in both directions with two sublayers. These two

sublayers compute forward and backward hidden sequences  $\vec{h}_t$  and  $\overleftarrow{h}_t$  respectively. Then, they are combined to compute the current hidden state  $h_t$  and the output of  $o_t$  and calculated as follows<sup>[56]</sup>.

$$\vec{h}_t = GRU(x_t, \vec{h}_{t-1}) \quad (13)$$

$$\overleftarrow{h}_t = GRU(x_t, \overleftarrow{h}_{t-1}) \quad (14)$$

$$h_t = W^T \vec{h}_t + W^V \overleftarrow{h}_t \quad (15)$$

$$o_t = \Phi(W^o h_t) \quad (16)$$

where GRU function represents the nonlinear transformation of the input vectors, which are encoded into the corresponding hidden state of GRU;  $W^T$  and  $W^V$  represent the weight coefficients corresponding to the forward hidden state  $\vec{h}_t$  and the reverse hidden state  $\overleftarrow{h}_t$  in the bidirectional GRU, respectively;  $W^o$  is the weight coefficient between the hidden and output layers.

BiGRU progressively encodes the entire molecular representation sequentially, with each bit in the ECFP corresponding to a specific substructure of the molecule. BiGRU controls the structure of the cyclic unit through its bi-directional gates, which are capable of focusing on both similarities and differences in the structure of the molecule.

## GCN

We encode each molecule as a molecular graph. Formally, represents the graph of the molecule, where is a set of  $n$  atomic nodes, and each node is represented by a 78 feature vector of atomic properties.  $E \in R_n \times n$  is the set of edges represented by the adjacency matrix of the molecular graph. The multi-layer graph convolution network (GCN) takes the node feature matrix  $X \in R^{N \times f}$  ( $N = |V|$ ,  $f$  represents the number of features of each node) and the adjacency matrix  $A \in R^{N \times N}$  as input, and then produces the node-level output  $Z \in R^{N \times F}$  ( $F$  represents the number of output features per node). For stability, the normalized propagation rule is defined as follows<sup>[52]</sup>.

$$H^{(l+1)} = \sigma \left( D^{-\frac{1}{2}} A D^{-\frac{1}{2}} H^{(l)} W^{(l)} \right) \quad (17)$$

where,  $A = A + I_N$  is the adjacency matrix of the undirected graph with added self-connections.  $D_{ii} = \sum_i A_{ii}$  is the diagonal node degree matrix.  $H^{(l)}$  and  $W^{(l)}$  are the learnable parameters of GCN and the output of the first layer respectively.  $\sigma(\cdot)$  is an activation function.

A layer-wise convolution operation can be approximated as follows<sup>[52]</sup>.

$$Z = D^{-\frac{1}{2}} A D^{-\frac{1}{2}} X \Theta \quad (18)$$

where  $\Theta \in R^{C \times F}$  ( $F$  is the number of filters of feature maps) is the matrix of filter parameters.

To better extract features, we designed two GCN layers, then used a global average pooling layer, and finally connected a fully connected layer. The GCN model helps in capturing graph feature information from the inputs.

## Fusion approach

Multimodal models not only require the construction of multimodal data, but the fusion of different modalities is also crucial. Multimodal fusion is the process of filtering, extracting, and combining required features from various sources of data. Currently, there are many available fusion methods including early fusion, late fusion, hybrid fusion, tensor fusion, hierarchical fusion, etc. Among them, late fusion is a commonly used method, which first processes each modality individually and then integrates their features at a higher level. Since each modality can learn its representation through independent processing, the model can better capture the specific features and relationships of each modality. Our model uses late fusion, as illustrated in Figure 2.

We use four machine learning methods and a gradient descent numerical algorithm to calculate the weights of the multi-modal model. To check the importance of the triple-modal model, the four machine learning methods are LASSO, ElasticNet, RF, and Gradient Boost, which are named Tri\_LASSO, Tri\_Elastic, Tri\_RF, Tri\_GB. To do it numerically, stochastic gradient descent (SGD), which is referred to as Tri\_SGD, is used to optimize the weights of multiple modal features.

$$O = \text{Concat}(O_{\text{Transformer-Encoder}}, O_{\text{BiGRU}}, O_{\text{GCN}}) \quad (19)$$

$$W_1, W_2, W_3 = \text{Weight}(O) \quad (20)$$

where  $O_{\text{Transformer-Encoder}}$ ,  $O_{\text{BiGRU}}$ , and  $O_{\text{GCN}}$  represent the outputs of the three feature extraction models, respectively, and  $O$  represent the tensor of fused molecular features.

$W_1, W_2$  and  $W_3$  represent the weights of the multi-modal model, and  $Weight(.)$  as a method of calculating the importance of the triple-modal model.

In the testing phase, each modal weight is multiplied with the newly calculated multimodal features to generate the final prediction value.

$$output = W_1 O'_{Transformer-Encoder} + W_2 O'_{BiGRU} + W_3 O'_{GCN} \quad (21)$$

where  $O'_{Transformer-Encoder}$ ,  $O'_{BiGRU}$  and  $O'_{GCN}$  represent the outputs of the three feature extraction models in the testing phase, respectively.

## Results and discussion

### Performance of single and multi-modal models

To verify the effectiveness of the multimodal model, we constructed both single models and multimodal models. The performance of the models was compared by calculating the root mean square error (RMSE), mean absolute error (MAE), and Pearson coefficient on the test set. As observed from the RMSE values in Table 2 and MAE values in Table 3, Tri\_LASSO, Tri\_Elastic, Tri\_RF, and Tri\_SGD have lower RMSE and MAE values than the best individual model except Delaney. The Tri\_SGD model has the lowest RMSE and MAE values among all tasks. Tri\_SGD is a robust fusion method that can effectively handle the characteristics of different data sets. As expected, multimodal learning can achieve better prediction than single-modal learning.

Table 2 RMSE performance of different data sets on 8 different models

Dataset	Delaney	Llinas2020	Lipophilicity	SAMPL	BACE	Warrior
Transformer	0.671	1.208	0.937	1.407	1.177	2.672
BiGRU	1.571	1.305	0.815	1.638	0.829	2.376
GCN	0.858	1.337	0.911	2.429	1.075	3.195
Tri_LASSO	0.811	1.193	0.782	1.099	0.981	2.337
Tri_Elastic	0.872	1.308	0.949	<b>1.103</b>	1.669	2.309
Tri_RF	0.804	1.173	0.848	1.341	0.978	2.215
Tri_GB	0.759	1.145	0.827	1.359	0.982	2.209
Tri_SGD	<b>0.620</b>	<b>1.065</b>	<b>0.725</b>	<b>1.103</b>	<b>0.762</b>	<b>2.164</b>

Table3 MAE performance of different data sets on 8 different models

Dataset	Delaney	Llinas2020	Lipophilicity	SAMPL	BACE	Warrior
Transformer	0.489	0.958	0.737	1.078	0.936	1.920
BiGRU	1.092	1.050	0.612	1.237	0.571	1.663
GCN	0.675	1.095	0.737	1.803	0.878	2.441
Tri_LASSO	0.568	0.955	0.616	0.855	0.770	1.706
Tri_Elastic	0.616	1.068	0.788	0.848	1.491	1.673
Tri_RF	0.613	0.933	0.639	1.00	0.723	1.562
Tri_GB	0.577	0.912	0.626	1.013	0.726	1.552
Tri_SGD	<b>0.470</b>	<b>0.844</b>	<b>0.565</b>	<b>0.822</b>	<b>0.530</b>	<b>1.540</b>

Pearson coefficient was calculated for the model results on the test sets. The Pearson coefficient represents the degree of agreement between the predicted value and the true value. As shown in Table 4, it can be observed that Tri\_SGD performs best on various tasks. Tri\_LASSO, Tri\_Elastic, Tri\_RF, Tri\_GB, and Tri\_SGD show consistent performance on the Llinas2020, Lipophilicity SAMPL, BACE and pKa Warrior datasets. The Tri\_SGD exhibited a notable improvement in the Llinas2020 and Lipophilicity datasets. Among single-modal learning, only Transformer can obtain comparable accuracy in Delaney and SAMPL datasets. Overall, Tri\_SGD achieved optimal values for RMSE, MAE, and Pearson coefficients across all tasks.

Table 4 Pearson coefficient performance of different data sets on 8 different models

Dataset	Delaney	Llinas2020	Lipophilicity	SAMPL	BACE	Warrior
Transformer	0.95	0.56	0.65	0.93	0.70	0.65
BiGRU	0.73	0.62	0.74	0.89	0.79	0.72
GCN	0.92	0.69	0.64	0.74	0.59	0.38
Tri_LASSO	0.94	0.67	0.75	<b>0.95</b>	0.75	0.75
Tri_Elastic	0.95	0.66	0.76	<b>0.95</b>	0.76	0.75
Tri_RF	0.93	0.66	0.72	<b>0.95</b>	0.75	0.75
Tri_GB	0.94	0.67	0.73	<b>0.95</b>	0.75	0.75
Tri_SGD	<b>0.96</b>	<b>0.73</b>	<b>0.79</b>	<b>0.95</b>	<b>0.82</b>	<b>0.76</b>

We calculated the cosine similarity between the true value and the predicted value of each model. The cosine similarity is to indicate the similarity between the predicted value and the true value. As shown in Figure 3, across different tasks, the cosine similarity of the true values and predicted values of Tri\_SGD is higher than that of any single models. Tri\_RF achieved the highest value in the SAMPL dataset, and Tri\_SGD is very close to Tri\_RF. The cosine similarity of Tri\_SGD reaches the highest value among other datasets.

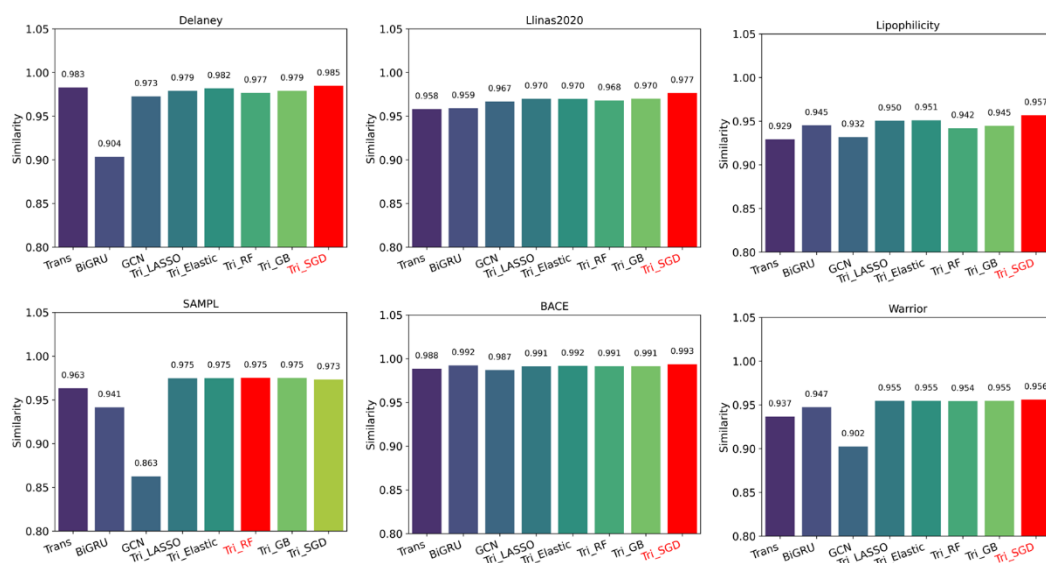


**Figure 3** Cosine similarity between true and predicted values. The highest similarity is highlighted in red color.

### Model reliability

To further evaluate the stability and reliability of the results, the model was repeated 15 times to calculate the Pearson coefficient distributions of the models. Multiple calculations of the Pearson coefficients provide a better reflection of the overall stability of the model's predictions. As shown in Figure 4, the performance of different mono-modal models vary greatly in the single-molecule datasets. For example, the Pearson coefficient of the Transformer-Encoder in Delaney reaches more than 0.90, while the Pearson coefficient of BiGRU is around 0.75. In addition, the performance of single modal models varies greatly across different datasets. The multimodal fusion method Tri\_SGD proposed in this study has the best Pearson coefficient across different datasets. Only Tri\_Elastic has the best Pearson coefficient value in the SAMPL dataset.

Overall, through 15 rounds of repeated calculations, The multimodal fusion method performs outstandingly in reliability. Especially, Tri\_SGD can significantly enhance the overall stability and reliability of the model, has better generalization ability, and is more adaptable to different data features.

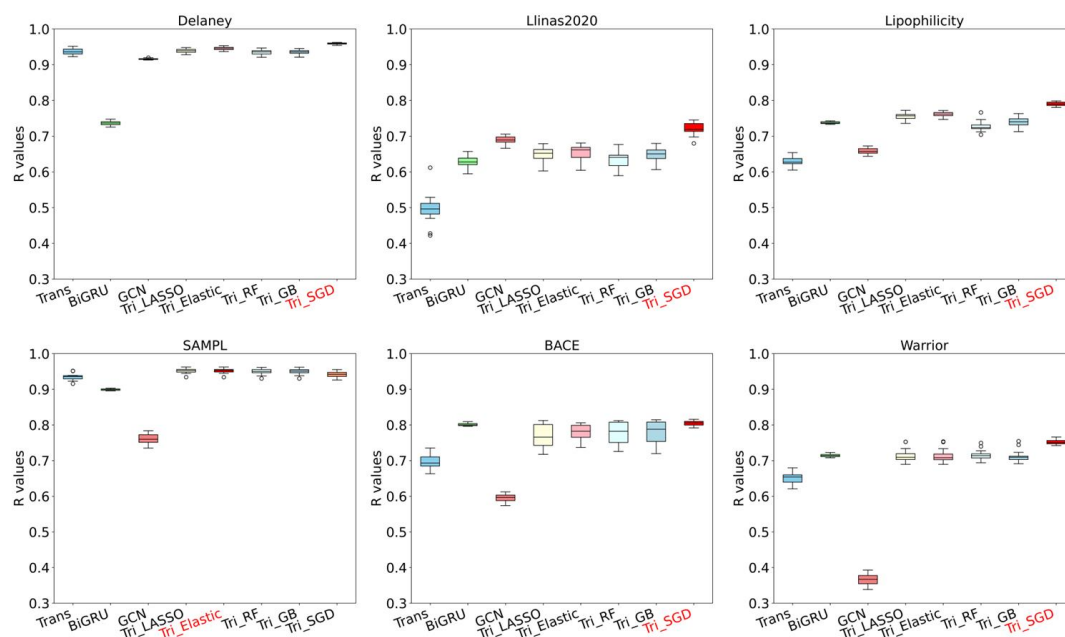


**Figure 4** Pearson coefficients of different datasets using three single-modal learning methods and five fused triple-modal learning methods.

## Feature distribution

To observe the relationship between the input features, we visualized the spatial distribution of SMILES-encoded vectors and ECFP fingerprints by using the dimensionality reduction method of uniform manifold approximation and projection (UMAP). Graph data is not suitable for dimensionality reduction because of its combined nodes and edges data format. The unmatched distribution between training and test set explains the poor performance of single-modal learning models. As shown in Figure 5, we find that SMILES-encoded vectors show well-overlapping spaces between the test set and the training set for four datasets other than the Llinas2020 and BACE datasets. Consistent with the RMSE results, Transformer does not obtain satisfactory RMSE and MAE on Llinas2020 and BACE dataset because the deep learning methods generally are better at interpolation than extrapolation. In Figure 6, the ECFP fingerprints did not overlap well between the training and test sets in SAMPL. Therefore, the RMSE of BiGRU is higher than that of Transformer in SAMPL. From UMAP, we can notice that the single molecular representation can represent parts of information. In some cases, the inability to achieve a consistent UMAP embedding space between the training and test sets has led to poorer predictive results on the test set. From molecular feature distribution, we can notice that the single modal learning models will tend to give poor performance if the test set does not well-overlap with the training set. In contrast, multi-modal learning still provides good performance in both Llinas2020 and BACE datasets than any single-modal learning models.

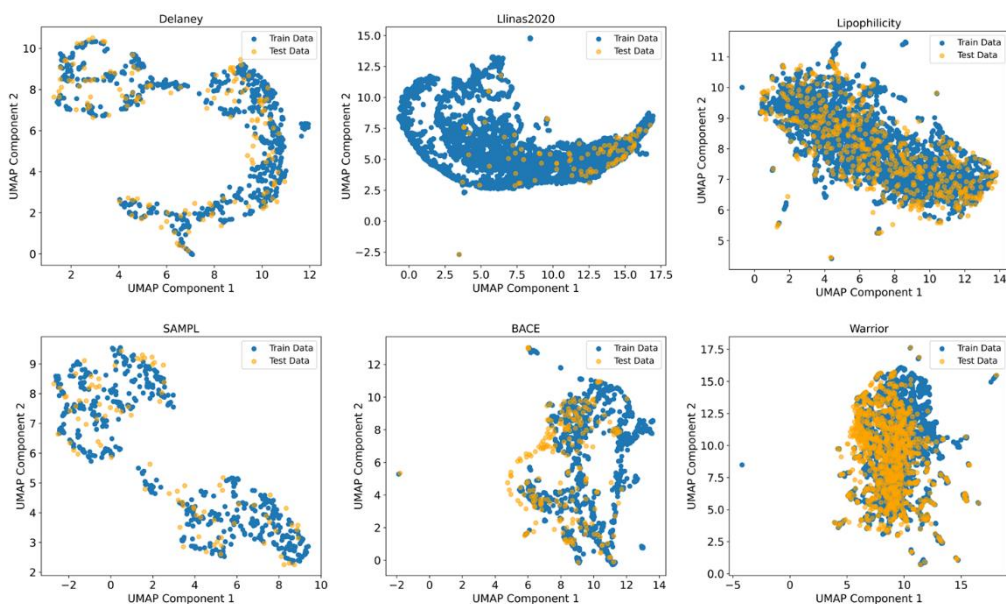


**Figure 5** UMAP diagram of SMILES-encoded vectors. Training and test dataset is colored in blue and orange. UMAP is fitted in the training dataset.

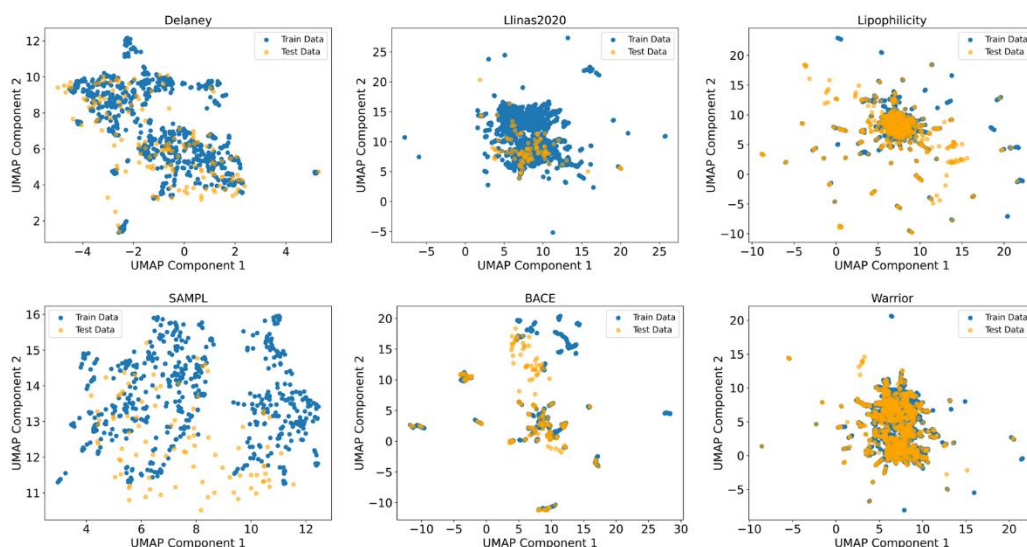


**Figure 6** UMAP diagram of ECFP. Training and test dataset is colored in blue and orange.

### Weights analysis in fusion

Some modalities may provide worse predictions than others in multi-modal learning. Therefore, the fusion is critical for the multi-model learning models. The perfect fusion should suppress the contribution from the weak modalities and encourage the contribution from informative modalities while keeping useful information. To explore the fusion capabilities, the weights of models after 15 rounds of iterations was averaged and shown in Figure 7. Tri\_LASSO, Tri\_Elastic, Tri\_RF, and Tri\_GB exhibited unbalanced weight allocations during the fusion process. Among them, the third feature (the weight for graph input from GCN) of Tri\_LASSO and Tri\_Elastic

even approaches to 0, meaning that no information is gained from graph data. Tri\_RF and Tri\_GB assigned the largest weights to models with SMILES-encoded vectors and ECFP, and the weight allocation on the third feature was relatively small. This unbalanced weight allocation may lead to insufficient consideration of Graph features, affecting the overall performance and generalization ability of the model. Tri\_SGD exhibited a more balanced weight allocation, as shown in Figure 7. The weight proportions for features of the first and third types of features are similar, and the weight ratio of the second type features is the highest. Overall, the Tri\_SGD fusion method makes full use of the three types of features, demonstrating the proper allocation strategy can enhance model accuracy and generalization ability.

Tri\_LASSO and Tri\_Elastic are linear regression methods, with Tri\_LASSO utilizing L1 regularization and Tri\_Elastic combining both L1 and L2 regularization. These regularization terms, in the presence of weakly correlated features in the data, may lead the feature weights to zero. SMILES-encoded vectors and ECFP fingerprints are sequence data and have a certain degree of correlation, so weights are assigned to these two types of features. Tri\_RF and Tri\_GB are nonlinear methods that can handle a certain degree of non-correlated information, but the weight assigned to the Graph feature is not sufficient. According to Figure 5 and Figure 6, in the Warrior dataset, the test set is well distributed in the space of the training set, and the performance of Tri\_LASSO, Tri\_Elastic, Tri\_RF, and Tri\_GB exceeds that of single modal models. Comparing the results among the five methods, we can find that neglecting one modal may lead to poorer performance. Tri\_SGD is an optimization algorithm that can effectively capture relationships of triple inputs. Though five fusion methods can improve the prediction performance, only Tri\_SGD can assign a more even weight distribution and show the best performance in each dataset. The results remind us that the proper fusion methods should not simply ignore the poor modal methods, and should take full utilization of complementary information from each modal input.

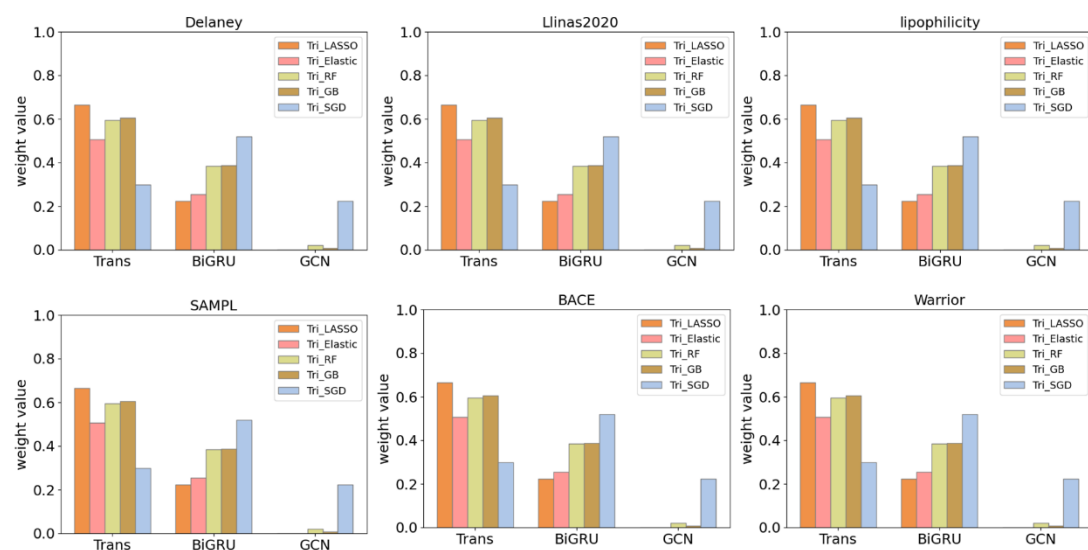


Figure 7 Weights distribution for each modal input of triple-modal learning methods in different datasets.

## Generalization ability validation

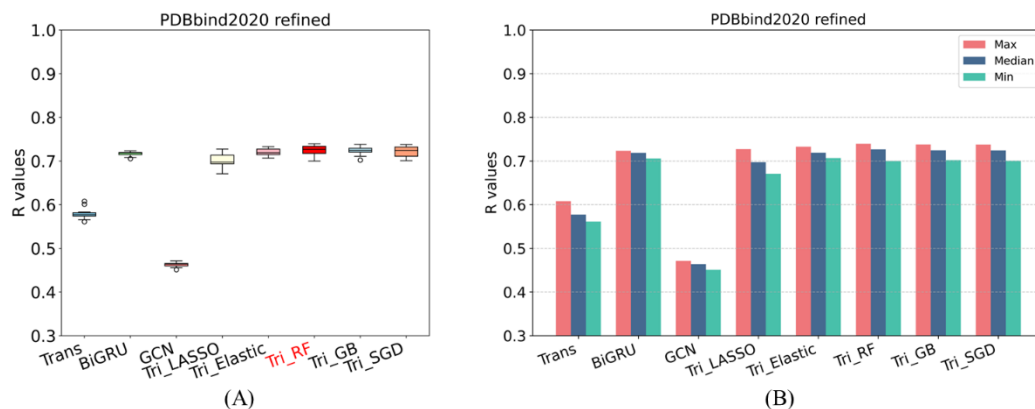
Our proposed multimodal fusion method achieved the best performance in single-molecule datasets of solubility, lipophilicity, inhibitory activity, and acidity/basicity. To verify the applicability of this method, we selected the refined set of PDBbind v2020 dataset for verification. As shown in Table 5, Tri\_Elastic has the minimum RMSE and MAE values, which are 1.349 and 1.048 respectively, but the results of Tri\_SGD are very close to the best results of Tri\_Elastic. Tri\_GB and Tri\_SGD achieved the best R value of 0.73. By leveraging multiple modalities, multi-modal learning can capture more diverse information compared to using a single modality. This enables the model to learn more comprehensive and robust representations of the data, leading to better generalization to unseen examples.

Table 5 Performance of RMSE, MAE, and Pearson on PDBbind2020 refined dataset

Dataset	RMSE	MAE	R
Transformer	1.807	1.420	0.56
BiGRU	1.388	1.073	0.72
GCN	1.986	1.570	0.64
Tri_LASSO	1.536	1.200	0.67
Tri_Elastic	<b>1.349</b>	<b>1.048</b>	0.72
Tri_RF	1.408	1.108	0.72
Tri_GB	1.400	1.101	<b>0.73</b>
Tri_SGD	1.358	1.067	<b>0.73</b>

To verify the stability of the multimodal model in the PDBbind2020 refined dataset, we also conducted 15 rounds of random seed testing. As observed in Figure 8(A) and Figure 8(B), the Pearson coefficient of single models in this dataset fluctuates, while the proposed multimodal fusion deep learning model shows relatively stable performance. The maximum, median, and minimum values of BiGRU, Tri\_Elastic, Tri\_RF, Tri\_GB, and Tri\_SGD all exceed 0.7. There are outliers in BiGRU and Tri\_GB. Generally, outliers will have a certain impact on the prediction results.

Combining the evaluation of RMSE, MAE, and R, the Tri\_SGD method demonstrates good accuracy and robustness on the PDBbind2020 refined dataset, and can better predict protein-ligand binding affinity. Notedly, we do not optimize the hyperparameters when applying our model to the PDBbind dataset and just extend the input dimension from the single-molecule dataset to protein-ligand complex molecules. In this study, we put our emphasis on the multi-modal learning methods and more accurate results would be reached after optimizing the models and selecting more proper inputs.



**Figure 8** Pearson coefficients of PDBbind2020 refined set. The box plot is the Pearson coefficient distribution in repeated learning, and the histogram plot is the maximum, median, and minimum values of the Pearson coefficient.

### Noise resistance capability of multimodal model

To verify the noise immunity of the model, we did a test on the SAMPL dataset by adding different noise levels of 0.05, 0.1, 0.2, and 0.5 to the input features of all the models. The error bar is computed from the 15 times repeated training. SMILES-encoded vectors add noise with random values from 1 to 34 (the maximum length of SMILES strings in SAMPL dataset), and ECFP fingerprints and graph feature vectors add noise with random values 0 or 1 at any bit positions. The experimental results are shown in Figure 9. Graph data is very sensitive to noise and it leads to the highest RMSE and MAE, and lowest Pearson coefficients after adding noise. The multimodal learning model shows remarkable noise resistance. We found that the Pearson coefficients of the multimodal fusion methods Tri\_LASSO, Tri\_Elastic, Tri\_RF, Tri\_GB, and Tri\_SGD are higher than those of the individual models when the noise is 0.1, 0.2, and 0.5. From the perspective of RMSE and MAE, the performance of Tri\_LASSO, Tri\_Elastic, Tri\_RF, and Tri\_GB is similar at different noise levels, while Tri\_SGD has the lowest RMSE and MAE values, indicating the proper fusion method can enhance the capability of noise resistance. The multi-modal fusion deep learning model demonstrates increased robustness in the presence of noisy data, with Tri\_SGD maintaining predictive accuracy while being more resilient to noise. The result indicates that fusion should not simply ignore the contribution from the weak modalities and proper fusion methods are required to keep useful information from each modal input.

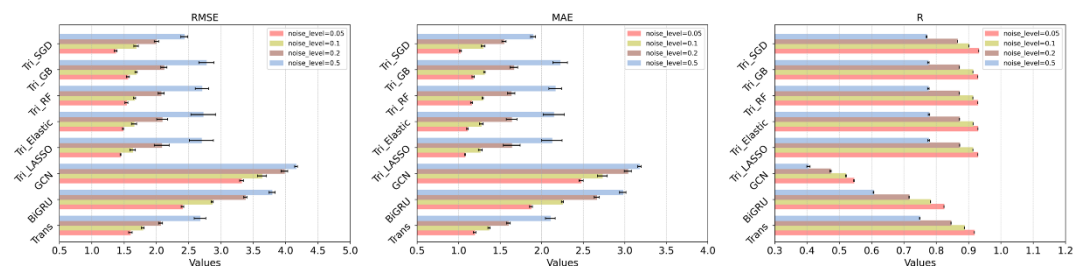


**Figure 9** RMSE, MAE, and R after adding different ratio of noise on the SAMPL dataset

## Conclusion

We construct a multimodal fused deep learning model that utilizes the complementary information of chemical language and molecular graphs to predict molecular properties. In this study, we applied SMILES-encoded vectors, ECFP, and graph to represent molecules, and adopted Transformer-Encoder, BiGRU, and GCN for each modal learning, respectively. We conducted comparisons on mono-modal and multimodal learning by using six single-molecule datasets, including solubility, lipophilicity, inhibitory activity, and acidity/basicity. The result indicates that the proposed multimodal fusion deep learning model not only improves the prediction accuracy and stability but also increases the ability of noise resistance by leveraging different sources of information. By assigning the proper weights in the fusion of triple modal features, the Tri\_SGD fusion method further improves the performance of multimodal learning models in dealing with uncorrelated data sources, such as chemical language and molecular graphs. Moreover, we demonstrate the generalization ability in predicting binding affinity for protein-ligand complex. We demonstrate that integrating information from different modalities can enhance model generalization capability in the case of data noise. Multimodal learning can be utilized to capture the complementarity between different modalities, which would benefit drug discovery.

## Funding

This work was supported by the National Natural Science Foundation of China (22003020, 62373172 and 12074151), the Natural Science Foundation of Jiangsu Province (BK20191032), and Changzhou Sci. & Tech. Program (CJ20200045), Postgraduate Research & Practice Innovation Program of Jiangsu Province (SJCX22\_1480).

## Declaration of competing interest

The authors declare that they have no known competing financial interests.

## Supplementary data

Supplementary data to this article can be found online.

## References

- [1] SCANNELL J W, BOSLEY J, HICKMAN J A, et al. Predictive validity in drug discovery: what it is, why it matters and how to improve it [J]. *Nature Reviews Drug Discovery*, 2022, 21(12): 915-31.
- [2] SATHE R Y, BHARATAM P V. Drug-dendrimer complexes and conjugates: Detailed furtherance through theory and experiments [J]. *Advances in colloid interface science*, 2022, 303: 102639.
- [3] LINCLAU B, WANG Z, JEFFRIES B, et al. Relating Conformational Equilibria to Conformer-Specific Lipophilicities: New Opportunities in Drug Discovery [J]. *Angewandte Chemie*, 2022, 134(7): e202114862.
- [4] MORITA K, HE S, NOWAK R P, et al. RETRACTED: Allosteric Activators of Protein Phosphatase 2A Display Broad Antitumor Activity Mediated by Dephosphorylation of MYBL2 [J]. *Cell*, 2020, 181(3): 702-15. e20.
- [5] FRACZKIEWICZ R, WALDMAN M. p K 50— A Rigorous Indicator of Individual Functional Group Acidity/Basicity in Multiprotic Compounds [J]. *Journal of Chemical Information Modeling*, 2023, 63(10): 3198-208.
- [6] RUBE H T, RASTOGI C, FENG S, et al. Prediction of protein–ligand binding affinity from sequencing data with interpretable machine learning [J]. *Nature biotechnology*, 2022, 40(10): 1520-7.
- [7] PARVATHANENI V, KULKARNI N S, MUTH A, et al. Drug repurposing: a promising tool to accelerate the drug discovery process [J]. *Drug discovery today*, 2019, 24(10): 2076-85.
- [8] FAN J, FU A, ZHANG L. Progress in molecular docking [J]. *Quantitative Biology*, 2019, 7: 83-9.
- [9] SALO-AHEN O M, ALANKO I, BHADANE R, et al. Molecular dynamics simulations in drug discovery and pharmaceutical development [J]. *Processes*, 2020, 9(1): 71.
- [10] LI J, LUO D, WEN T, et al. Representative feature selection of molecular descriptors in QSAR modeling [J]. *Journal of Molecular Structure*, 2021, 1244: 131249.
- [11] TROTT O, OLSON A J. AutoDock Vina: improving the speed and accuracy of docking with a new scoring function, efficient optimization, and multithreading [J]. *Journal of computational chemistry*, 2010, 31(2): 455-61.
- [12] LECUN Y, BENGIO Y, HINTON G. Deep learning [J]. *nature*, 2015, 521(7553): 436-44.
- [13] KIM H K, MIN S, SONG M, et al. Deep learning improves prediction of CRISPR–Cpf1 guide RNA activity [J]. *Nature biotechnology*, 2018, 36(3): 239-41.
- [14] DENG J, YANG Z, OJIMA I, et al. Artificial intelligence in drug discovery: applications and techniques [J]. *Briefings in Bioinformatics*, 2022, 23(1): bbab430.
- [15] HASSELGREN C, OPREA T I. Artificial Intelligence for Drug Discovery: Are We There Yet? [J]. *Annual Review of Pharmacology and Toxicology*, 2023.
- [16] MA J, SHERIDAN R P, LIAW A, et al. Deep neural nets as a method for quantitative structure–activity relationships [J]. *Journal of chemical information modeling*, 2015, 55(2): 263-74.
- [17] KARIMI M, WU D, WANG Z, et al. DeepAffinity: interpretable deep learning of compound–protein affinity through unified recurrent and convolutional neural networks [J]. *Bioinformatics*, 2019, 35(18): 3329-38.
- [18] GAO F, SHEN Y, SALLACH J B, et al. Direct prediction of bioaccumulation of organic

- contaminants in plant roots from soils with machine learning models based on molecular structures [J]. *Environmental Science Technology*, 2021, 55(24): 16358-68.
- [19] GILMER J, SCHOENHOLZ S S, RILEY P F, et al. Neural message passing for quantum chemistry; proceedings of the International conference on machine learning, F, 2017 [C]. PMLR.
- [20] TANG B, KRAMER S T, FANG M, et al. A self-attention based message passing neural network for predicting molecular lipophilicity and aqueous solubility [J]. *Journal of cheminformatics*, 2020, 12(1): 1-9.
- [21] WITHNALL M, LINDELÖF E, ENGVIST O, et al. Building attention and edge message passing neural networks for bioactivity and physical-chemical property prediction [J]. *Journal of cheminformatics*, 2020, 12(1): 1-18.
- [22] KEARNES S, GOLDMAN B, PANDE V. Modeling industrial ADMET data with multitask networks [J]. arXiv preprint arXiv:170310603, 2016.
- [23] XIE L, XU L, KONG R, et al. Improvement of Prediction Performance With Conjoint Molecular Fingerprint in Deep Learning [J]. *Frontiers in Pharmacology*, 2020, 11.
- [24] XIE L, XU L, CHANG S, et al. Multitask deep networks with grid featurization achieve improved scoring performance for protein-ligand binding [J]. *Chemical biology & drug design*, 2020, 96(3): 973-83.
- [25] WENZEL J, MATTER H, SCHMIDT F. Predictive Multitask Deep Neural Network Models for ADME-Tox Properties: Learning from Large Data Sets [J]. *Journal of Chemical Information and Modeling*, 2019, 59(3): 1253-68.
- [26] KWON S, BAE H, JO J, et al. Comprehensive ensemble in QSAR prediction for drug discovery [J]. *BMC Bioinformatics*, 2019, 20(1): 521.
- [27] RAMSUNDAR B, LIU B, WU Z, et al. Is Multitask Deep Learning Practical for Pharma? [J]. *Journal of Chemical Information and Modeling*, 2017, 57(8): 2068-76.
- [28] BALTRUŠAITIS T, AHUJA C, MORENCY L-P. Multimodal machine learning: A survey and taxonomy [J]. *IEEE transactions on pattern analysis and machine intelligence*, 2018, 41(2): 423-43.
- [29] STAHLSCHMIDT S R, ULFENBORG B, SYNNERGREN J. Multimodal deep learning for biomedical data fusion: a review [J]. *Briefings in Bioinformatics*, 2022, 23(2): bbab569.
- [30] YUAN W, CHEN G, CHEN C Y-C. FusionDTA: attention-based feature polymerizer and knowledge distillation for drug-target binding affinity prediction [J]. *Briefings in Bioinformatics*, 2022, 23(1): bbab506.
- [31] TANOORI B, JAHROMI M Z, MANSOORI E G. Drug-target continuous binding affinity prediction using multiple sources of information [J]. *Expert Systems with Applications*, 2021, 186: 115810.
- [32] JIANG D, WU Z, HSIEH C-Y, et al. Could graph neural networks learn better molecular representation for drug discovery? A comparison study of descriptor-based and graph-based models [J]. *Journal of cheminformatics*, 2021, 13(1): 1-23.
- [33] DONG W, YANG Q, WANG J, et al. Multi-modality attribute learning-based method for drug-protein interaction prediction based on deep neural network [J]. *Briefings in Bioinformatics*, 2023, 24(3): bbad161.
- [34] SUN H, WANG J, WU H, et al. A Multimodal Deep Learning Framework for Predicting PPI-Modulator Interactions [J]. *Journal of Chemical Information and Modeling*, 2023, 63(23): 7363-72.

- [35] D'MELLO S K, KORY J. A review and meta-analysis of multimodal affect detection systems [J]. *ACM computing surveys (CSUR)*, 2015, 47(3): 1-36.
- [36] SNOEK C G, WORRING M, SMEULDERS A W. Early versus late fusion in semantic video analysis; proceedings of the Proceedings of the 13th annual ACM international conference on Multimedia, F, 2005 [C].
- [37] ATREY P K, HOSSAIN M A, EL SADDIK A, et al. Multimodal fusion for multimedia analysis: a survey [J]. *Multimedia systems*, 2010, 16: 345-79.
- [38] DIETTERICH T G. Ensemble methods in machine learning; proceedings of the International workshop on multiple classifier systems, Berlin, F, 2000 [C]. Heidelberg: Springer Berlin Heidelberg.
- [39] NEVEROVA N, WOLF C, TAYLOR G, et al. Moddrop: adaptive multi-modal gesture recognition [J]. *IEEE Transactions on Pattern Analysis and Machine Intelligence*, 2015, 38(8): 1692-706.
- [40] LIU K, LI Y, XU N, et al. Learn to combine modalities in multimodal deep learning [J]. *arXiv preprint arXiv:180511730*, 2018.
- [41] YANG X, NIU Z, LIU Y, et al. Modality-DTA: Multimodality Fusion Strategy for Drug-Target Affinity Prediction [J]. *IEEE/ACM Trans Comput Biol Bioinform*, 2023, 20(2): 1200-10.
- [42] DEHGHAN A, RAZZAGHI P, ABBASI K, et al. TripletMultiDTI: Multimodal representation learning in drug-target interaction prediction with triplet loss function [J]. *Expert Systems with Applications*, 2023, 232: 120754.
- [43] WU Z, RAMSUNDAR B, FEINBERG E N, et al. MoleculeNet: a benchmark for molecular machine learning [J]. *Chemical science*, 2018, 9(2): 513-30.
- [44] SANDER T, FREYSS J, VON KORFF M, et al. DataWarrior: an open-source program for chemistry aware data visualization and analysis [J]. *Journal of chemical information and modeling*, 2015, 55(2): 460-73.
- [45] FRANCOEUR P G, KOES D R. SolTranNet—A machine learning tool for fast aqueous solubility prediction [J]. *Journal of chemical information and modeling*, 2021, 61(6): 2530-6.
- [46] WEININGER D. SMILES, a chemical language and information system. 1. Introduction to methodology and encoding rules [J]. *Journal of chemical information and computer sciences*, 1988, 28(1): 31-6.
- [47] JAMES C A. OpenSMILES specification [J]. A: OpenSMILES, 2016.
- [48] ROGERS D, HAHN M. Extended-connectivity fingerprints [J]. *Journal of chemical information and modeling*, 2010, 50(5): 742-54.
- [49] AVRAM S, BORA A, HALIP L, et al. Modeling kinase inhibition using highly confident data sets [J]. *Journal of Chemical Information and Modeling*, 2018, 58(5): 957-67.
- [50] SAWADA R, KOTERA M, YAMANISHI Y. Benchmarking a Wide Range of Chemical Descriptors for Drug-Target Interaction Prediction Using a Chemogenomic Approach [J]. *Molecular informatics*, 2014, 33(11-12): 719-31.
- [51] AXEN S D, HUANG X-P, CÁ CERES E L, et al. A simple representation of three-dimensional molecular structure [J]. *Journal of medicinal chemistry*, 2017, 60(17): 7393-409.
- [52] NGUYEN T, LE H, QUINN T P, et al. GraphDTA: Predicting drug–target binding affinity with graph neural networks [J]. *Bioinformatics*, 2021, 37(8): 1140-7.
- [53] VASWANI A, SHAZEER N, PARMAR N, et al. Attention is all you need [J]. *Advances in neural information processing systems*, 2017, 30.

- [54] YAN H, DENG B, LI X, et al. TENER: adapting transformer encoder for named entity recognition [J]. arXiv preprint arXiv:04474, 2019.
- [55] CHUNG J, GULCEHRE C, CHO K, et al. Empirical evaluation of gated recurrent neural networks on sequence modeling [J]. arXiv preprint arXiv:, 2014.
- [56] LIN X, QUAN Z, WANG Z-J, et al. A novel molecular representation with BiGRU neural networks for learning atom [J]. 2020, 21(6): 2099-111.